Biomaterials Advances 180 (2026) 214601

Contents lists available at ScienceDirect

Biomaterials Advances

journal homepage: www.journals.elsevier.com/materials-science-and-engineering-c

Gelatin and collagen-mimetic nanoparticles for intraperitoneal cisplatin delivery: From synthesis to *in-vivo* SPECT imaging of biodistribution

Xenia Kovalyk [a,b,c], Sven Saniternik [a,b,c], Larissa-M. Hamacher [a,b,c], Ben Lasse Mink [a,b], Sven Thoröe-Boveleth [d], Patricia Bach [b], Thomas Endres [e], Maria Montero-Mirabet [e], Annette M. Schmidt [b], Holger Grüll [a,b,c,*]

[a] University of Cologne, Faculty of Medicine and University Hospital Cologne, Department of Diagnostic and Interventional Radiology, 50937, Cologne, Germany
[b] University of Cologne, Department of Chemistry and Biochemistry, 50939, Cologne, Germany
[c] University of Cologne, Faculty of Medicine and University Hospital Cologne, Core Facility Experimental and Preclinical Imaging Cologne, 50937, Cologne, Germany
[d] Institute for Occupational, Social and Environmental Medicine, Medical Faculty, RWTH Aachen University Hospital, Aachen, 52074, Germany
[e] Evonik Operations GmbH, Health Care, 64293, Darmstadt, Germany

A B S T R A C T

Peritoneal carcinomatosis is a metastatic condition with poor prognosis, commonly associated with abdominal cancers. Current treatments comprise cytoreductive surgery with systemic chemotherapy or may include more invasive options such as hyperthermic intraperitoneal chemotherapy, and pressurized intraperitoneal aerosol chemotherapy. However, currently, all treatment options are considered palliative as remaining cancer cells cause recurrence. This study explores new intraperitoneal drug delivery systems based on gelatin-poly(glutamic acid) (Gel-PGA-NPs) or collagen-like-peptide-poly(glutamic acid) nanoparticles (CLP-PGA-NPs) loaded with cisplatin for localized treatment of peritoneal carcinomatosis. These NPs, synthesized *via in situ* polymerization, offer prolonged drug release and continuous biodegradation. The used CLP is produced by a recombinant manufacturing method avoiding any animal-derived material, which has advantages in regard to biocompatibility and reproducibility. Characterization by dynamic light scattering and transmission electron microscopy showed NPs averaging 150 nm in size. Cisplatin loading in CLP-PGA NPs facilitated high drug loading and stability compared to Gel-PGA NPs. SPECT/CT imaging of radiolabeled NPs in healthy mice revealed primary uptake in the spleen and liver, and further accumulation in the pancreas, ovaries and adherence to abdominal tissues highlighting the potential use for treatment of intraperitoneal metastases.

1. Introduction

Peritoneal carcinomatosis (PC) is a complex disease characterized by the metastatic spread of cancer cells to the peritoneum, the serous membrane lining the abdominal cavity and enveloping the abdominal organs. This condition is often diagnosed in patients with advanced-stage malignancies, particularly cancers originating in the gastrointestinal tract, such as ovarian, colorectal, pancreatic, and gastric cancers among others.

The incidence of PC is estimated to be up to 14 % for pancreatic cancer, approximately 11 % for colorectal cancer, around 14–50 % for gastric cancer, and as high as 70 % for ovarian cancer [1–4]. The presence of PC often reflects poor prognosis, indicating a widespread disease mostly without curative approaches. Treatment options at this advanced stage comprise cytoreductive surgery often followed by hyperthermic intraperitoneal chemotherapy (HIPEC) or pressurized intraperitoneal aerosol chemotherapy (PIPAC) alongside with further systemic chemotherapy. However, treatment aims at life extension and reduction of symptoms but is considered as palliative care due to recurrence originating from remaining cancer cells [5]. One of the major challenges in treating PC is the poor perfusion of surface tumors, which are often poorly connected to the main vascular system. As a result, these tumors are less responsive to conventional intravenous (IV) chemotherapy. Intraperitoneal (IP) drug delivery has been proposed as a promising strategy to improve localized drug exposure to peritoneal metastases. IP administration of drug delivery systems (DDSs) offers the advantage of longer residence time and thus provides an extended and more direct exposure to drugs compared to IV administration.

Post-operative treatment of remaining cancer cells with IP drug delivery is currently explored in first clinical trials and is subject of research in a preclinical setting [6–11]. As of today, no formulation has been specifically approved for IP delivery [12]. Earlier research has

* Corresponding author at: University of Cologne, Faculty of Medicine and University Hospital Cologne, Department of Diagnostic and Interventional Radiology, 50937, Cologne, Germany.
E-mail address: holger.gruell@uk-koeln.de (H. Grüll).

https://doi.org/10.1016/j.bioadv.2025.214601
Received 8 August 2025; Received in revised form 5 November 2025; Accepted 6 November 2025
Available online 16 November 2025

shown that tumor-targeting as well as tumor penetration, but also clearance from the intraperitoneal space of drug-loaded nano- and microparticles after IP administration depend on size and possibly on other material properties such as surface charge and coatings [13]. Particle-based DDSs have been studied with sizes between 50 nm to several microns in small animal models of PC. Tumor uptake was mainly assessed using *ex vivo* histological examination [14–16]. The findings are diverse and do not allow to conclude on the most suited diameter or surface properties. The choice of drug primarily depends on the type of primary tumor, with cis-diaminodichloroplatinum (cisplatin, CDDP), doxorubicin (DOX), and paclitaxel (PTX) being commonly used in clinical applications of IP chemotherapy [17–19]. Particularly, IP administration of platinum-based chemotherapeutics such as CDDP showed promising results in patients with gynecological cancers or in combination with mitomycin C for colorectal cancers [20,21]. However, due to their molecular size (smaller than 2 nm), these chemotherapeutic drugs are rapidly eliminated from the peritoneal cavity *via* blood vessels [22]. The use of sustained-release DDSs with large diameters could help maintain adequate drug exposure to residual tumor cells within the peritoneal cavity [23–25].

CDDP is one of the most potent drugs for treatment of several abdominal or gynecological tumors and is used for HIPEC treatments as well [21]. One of the disadvantages of CDDP is its poor solubility in water as well as organic solvents such as dimethylformamide (DMF) or dimethylsulfoxide (DMSO) making synthesis of DDSs with sufficient CDDP payload challenging. However, the use of DMSO during synthesis is strongly discouraged as it inserts into the complex as a ligand [26]. The strategy to simply entrap CDDP in polymeric nanoparticles (NPs) suffers from low encapsulation efficiency and yields systems with poor release profiles [27,28]. A better option is the chemical complexation of CDDP by amphiphilic block copolymers that contain carboxylic groups, leading to micellar structures with polymer-metal complexes which may improve the drug release profile and increase the drug load [29,30].

These typically core-shell-structured polymeric micelles can be fabricated *via* self-assembly procedures. However, they require a block copolymer precursor, which entails time-intensive and complex synthesis procedures. In past studies, advantage was taken of the simultaneous polymerization and self-assembly between the components for development of a more facile procedure using macromolecules as template [31]. This approach is based on polymerization of monomers in a biopolymer-monomer pair reaction system consisting of biopolymer and polymerizable monomer. Particularly, gelatin was studied as template and acrylic acid (AA) as monomer for polymerization of AA in the gelatin aqueous solution. Stable core-shell NPs with multiple functional groups were obtained [31]. In subsequent studies by *Ding* et al., incorporation of CDDP into these gelatin-poly (acrylic acid) (Gel-PAA) NPs through the interaction between platinum of CDDP and carboxylic groups in the NPs was investigated [32–34]. The NPs, which contain many carboxyl groups from both gelatin and PAA, enable high CDDP loading with an encapsulation efficiency up to 70 %. In addition, a slow-release drug profile with a small initial burst of only 13–28 % after 8 h is found [32]. These particles showed promising efficacy after IV and IP injection in a subcutaneous model of hepatocellular carcinoma [32,34].

Here, we present a novel DDS based on gelatin-poly(glutamic acid) particles (Gel-PGA-NPs) loaded with CDDP. Poly(glutamic acid) (PGA) has been extensively studied in drug delivery and cosmetic applications and is considered a biocompatible, safe and non-toxic building block [35,36]. Furthermore, PGA has been used as a drug carrier for loading with CDDP, demonstrating its application in drug delivery [37,38]. Previous gelatin–PGA systems have been tested mostly as glues, scaffolds, hydrogels and occasionally particles, relying on the physical mixing of pre-formed gelatin and PGA polymers [39–42]. These systems often suffered from poor stability. To address this, recent studies have attempted to improve stability through external crosslinking [43–45]. PGA is biodegradable and avoids potential toxicity compared to PAA and its monomer AA, especially when considering the need for an external initiator for the polymerization such as potassium persulfate [46–50]. Next to animal-derived gelatin, we use a new type of collagen-like-peptide (CLP) marketed under the brand Vecollan®, which is obtained *via* advanced recombinant protein production. Vecollan® contains no animal- or human-derived ingredients and has precisely defined chemical properties such as molecular weight and amino acid sequence translating into more defined synthesis procedures and particles with narrower size distribution [51,52]. These well-defined chemical properties and its vegan production methods are beneficial for clinical translation from a regulatory perspective.

In this article, we present the synthesis, characterization and release profiles in fetal bovine serum (FBS) of CDDP-loaded Gel-PGA-NPs in comparison to CDDP-loaded CLP-PGA-NPs. Moreover, we present the *in vivo* biodistribution of radiolabeled CLP-PGA-NPs after injection into the peritoneal cavity using single-photon emission computed tomography (SPECT/CT) imaging in healthy animals. Longitudinal imaging is crucial to gain an understanding of the relationship between the physicochemical properties of particle-based carriers and their biological fate following IP administration. This article establishes the methodology and baseline that will be used in future therapeutic studies in tumor-bearing animals.

2. Experimental section

2.1. General/materials

All solvents were obtained from *Sigma-Aldrich* (St Louis, MO, USA). Type-B gelatin with 100–115 mmol of carboxylic acid per 100 g of protein and an isoelectric point (pI) of 4.7–5.2 were purchased from *Sigma-Aldrich* (St Louis, MO, USA) with an average molecular weight of 20,000–25,000 g/mol (50–120 bloomstrength). Gelatin was refined once by dissolving it in distilled water followed by precipitating with acetone and drying at room temperature. Vecollan®, a recombinantly manufactured CLP, was kindly provided by *Evonik Operations GmbH* (Essen, Germany). CDDP was purchased from *TCI Chemicals* (Tokyo, Japan). *N*-tert-butoxycarbony-*L*-glutamic acid gamma-benzyl ester (Boc-(*L*)Glu(OBzl)-OH, ≥98 % purity) and propanephosphonic acid anhydride (T3P®, 50 % solution in ethyl acetate) were purchased from *Sigma-Aldrich*. All reagents were used as received from commercial sources without further purification. Water was purified using a Milli-Q system by *Sartorius*. A *Hereaus* Multifuge 3 SR Plus and *Eppendorf* Centrifuge 5425 (Wesseling, Germany) centrifuges were used for centrifugation. [^{111}In]$InCl_3$ was acquired from *Curium* (Petten, Netherlands) as a solution in 0.02 M hydrochloric acid (HCl) (usually 185 MBq in approx. 500 μl).

2.2. Synthesis of Gel-PGA and CLP-PGA NPs

2.2.1. Preparation of (S)-glutamic acid 5-benzyl ester-N-carboxyanhydride

(*S*)-glutamic acid 5-benzyl ester N-carboxyanhydride ((*S*)Glu(OBzl)-NCA) was synthesized in a single step following a procedure adapted from *Laconde* et al. [53] Under an inert atmosphere, Boc-(*L*)Glu(OBzl)-OH (25 g) was dissolved in ethyl acetate (150 ml). A solution of T3P® (1.2 eq) in ethyl acetate was added dropwise followed by pyridine (1 eq.). The mixture was stirred at room temperature for 2 h. Subsequently, ice-cold water (100 ml) was added. The organic layer was separated, washed twice with a cold saturated NaCl solution (2 × 50 ml), and then dried over $MgSO_4$. After filtration, the solvent was removed under reduced pressure obtaining a colorless solid. Diethylether (100 ml) was added to the colorless residue. Recrystallization from diethylether followed by filtration yielded (*S*)Glu(OBzl)-NCA as colorless crystals which were stored under argon atmosphere at 4 °C. Yield: 71 %. NMR data matched the literature [54].

^{1}H NMR (300 MHz, $CDCl_3$): δ 7.35 (m, 5H), 6.80 (s, 1H), 5.13 (s, 2H), 4.38 (t, 1H), 2.58 (t, 2H), 2.32–2.11 (m, 2H).

^{13}C NMR (75 MHz, $CDCl_3$): δ 172.47, 169.58, 152.25, 135.37,

128.81, 128.66, 128.43, 67.17, 56.96, 29.77, 26.94.

2.2.2. Preparation of Gel-PGA and CLP-PGA NPs

Synthesis was based on a procedure described by *Ding* et al. [33] Purified gelatin (0.35 g) or CLP (0.35 g) was dissolved in 50 ml of purified water. *(S)*Glu(OBzl)-NCA (0.1 g for gelatin-based and 0.085 g for CLP-based NPs) was dissolved in 4 ml DMF and cooled in an ice bath. The organic solution was slowly added over a dropping funnel. The polymerization of *(S)*Glu(OBzl)-NCA monomer was initiated by the amino groups of gelatin obtaining poly((*S*)-5-benzylglutamate) (PBLG). As opalescence appeared in the reaction mixture, which was a signal for nanoparticle formation, the reaction was allowed to proceed for another 15 min at room temperature. The resultant suspension was then filtered to remove any larger aggregates and dialyzed against water for 24 h using a dialysis membrane bag (12,000 Da molecular weight cutoff) to remove residual monomers. Deprotection of carboxy groups of PBLG was conducted according to an adjusted procedure by *Conejos-Sánchez* et al. [54]. In a round bottom flask, to benzyl-protected Gel-PBLG NPs in aqueous solution, 2 equiv. of NaOH per carboxylic group of the PBLG block was added in 2 ml of purified water. The mixture was stirred overnight for 16 h. The deprotected NPs were again dialyzed against distilled water for 24 h. Subsequently, the crosslinking reaction of the NPs was conducted by adding the desired amount of 2,2′-(ethylenedioxy)-bis(ethylamine) (EDEA) as crosslinker in the presence of EDC at room temperature for 8 h. The crosslinker to carboxy group ratio amounted to 1:2. The EDC to crosslinker ratio was 0.5:1. The crosslinked product was again dialyzed against distilled water for 24 h.

2.2.3. Preparation of CDDP-loaded Gel-PGA and CLP-PGA NPs

CDDP was added to an aqueous suspension of CLP-PGA NPs in a ratio of 2:1 of CDDP to carboxy groups in NPs. The resultant mixture was shaken at 400 rpm at 37 °C for two days. The unbound CDDP was removed by dialysis against distilled water using a 12,000 Da molecular weight cutoff dialysis membrane for two days.

2.2.4. Radiolabeling of CLP-PGA NPs

For labeling experiments, 10 mg of the CLP-based NPs were lyophilized and redispersed in 0.25 ml of 1 M sodium acetate buffer in a 1.5 ml reaction vial. 0.25 ml of [^{111}In]$InCl_3$ (100 MBq) was added to the reaction vial resulting in a solution with pH ~ 5. The labeling mixture was incubated at 37 °C for 120 min. To verify the stability of the nanoparticle complex, 5 μl of the competing chelating agent diethylenetriaminepentaacetic acid (DTPA; 10 mM) was added and incubated for 10 min at 37 °C. The ^{111}In-labeled NPs were separated from unbound [^{111}In]In^{3+} or DTPA-complexed radionuclides using a PD MiniTrap G-25 Sephadex column (*GE Healthcare*, Uppsala, Sweden) eluted with physiological saline solution. The radiochemical purity and yield were determined by thin layer chromatography (radio-TLC) on silica plates. Mobile phase consisted of 0.1 M citrate buffer. The exposed plates were analyzed on a FLA-7000 phosphor imager (*FujiFilm*, Tokyo, Japan) using the AIDA software. Radiochemical purity and yield were determined.

2.3. Characterization

The hydrodynamic diameter, polydispersity of nano-sized particles and surface potential was determined using a Zetasizer Nano ZS (*Malvern Panalytical Ltd.*, Malvern, UK). No further filtrations of the particles were performed throughout the entire experiment. In between measurements the samples were stored at 4 °C. TEM images were recorded on electron microscopes (Talos L120C, *ThermoFisher*, Waltham, USA and Leo 912, *Zeiss*, Oberkochen, Germany). Samples were prepared by placing the dispersion (3 μl) on a 300-mesh carbon-coated copper grid and letting it dry at room temperature. NMR spectra were recorded on a *Bruker* Avance II spectrometer operating at 300 MHz using deuterated solvents. For measuring the CDDP content, 1 ml of rhodium solution (1 mg/l) was added to the samples as an internal standard and then destroyed upon heating in fuming nitric acid (≥ 99 %). After filtration with a 0.2 μl syringe filter, the Pt concentration in the solution was determined by inductively coupled plasma mass spectrometry (ICP-MS, 8900-QQQ, *Agilent*, Waldbronn, Germany). Measurements were carried out under following conditions: A MicroMist quartz glass Meinhard nebulizer was used. The RF power was set to 1550 W, the plasma flow was adjusted to 15 l/min and the nebulizer flow was set to 1.15 l/min. A 2-mm quartz glass injector was employed.

2.4. In vitro drug release

NPs were dispersed at a concentration of 0.1 mg CDDP/ml in 1.5 ml of fetal bovine serum (FBS, pH 7.4) and incubated at 37 °C under shaking. At determined time intervals, the vials were centrifuged at 10000 rpm for 20 min. 0.5 ml of supernatant was taken and analyzed by ICP-MS as described in Section 2.3. Equal volume of FBS was replaced. Studies were carried out in duplicate.

2.5. In vitro toxicity studies

Colorectal cancer (CT26) cells were grown in DMEM supplemented with 10 % FBS and 1X Penicillin/Streptomycin. The cells were cultured in flasks at 37 °C in an atmosphere of 95 % air and 5 % CO_2, in an incubator. Cells were plated in 96-well plates at the density of 2000 viable cells per well in 0.2 ml of complete DMEM medium and incubated 24 h. The total cell counts, and viability were counted by the trypan blue dye exclusion method. The cells were incubated with CDDP, CDDP-loaded NPs and drug-free control NPs (in the same amount of weight as drug-loaded NPs for comparison) for 48 and 72 h. After treatment, the formulations were replaced with 40 μl of a 5 mg/ml thiazolyl blue tetrazolium bromide solution (MTT) in PBS and cells were then incubated for an additional 3 h. The resulting formazan crystals were solubilized by the addition of 150 μl DMSO. Absorbance was measured at 570 nm using an Epoch microplate reader (*Agilent*, Waldbronn, Germany). The results were expressed as mean values with standard deviation of three measurements.

2.6. In vivo biodistribution

All animal experiments were approved by the Federal Ministry of Agriculture, Food and Homeland of North-Rhine Westphalia (BMLEH, animal ethical proposal no.: 81–02.04.2020.A320). Healthy Balb/c mice (8 weeks old, 19–22 g, *Charles River*, USA) were IP injected with ^{111}In-labeled CLP-PGA NPs (23.7 ± 0.6 MBq in 0.2 ml per animal of a 20 mg/ml NP dispersion in isotonic 0.9 % NaCl solution) and imaged using SPECT/CT. On injection day, the animals were imaged sequentially for 4 h with scans performed every 30 min. Subsequent imaging occurred daily for seven days, after which the animals were sacrificed. Following pharmacokinetic studies, biodistribution was determined by dissecting the animals, weighing, and isolating the respective tissues (blood, mediastinal lymph nodes (LNs), urine, head, femur muscle, small intestines, colon, stomach, stomach content, femur bone, skin, kidneys, liver, pancreas, spleen, heart, lung, bladder, ovaries, mesentery, peritoneum, brain). Tissue radioactivity was quantified using gamma-counting. All presented data are decay-corrected. The particle distribution was studied using autoradiography, on 10 μm slices of cryogenically embedded samples. The relative distribution was normalized to the tissue exhibiting the highest signal per unit area. Therefore, a circular region of interest (ROI) with an area of 1.2 mm^2 was selected for quantification.

2.7. Longitudinal SPECT/CT

After IP injection of the radiolabeled particles, one SPECT image per hour was acquired over 4 h total (scan parameters: 25 s/projection, 12 projections, 100.0 mm axial FOV; nanoSPECT®, *Mediso*, Budapest,

Hungary). From day one to seven, one scan per day was acquired using the same settings. After the last scan, mice were sacrificed for autoradiographic and biodistribution analysis. Images were evaluated with Imalytics Preclinical® (*Gremse-IT,* Germany) [55]. All presented data are decay-corrected.

3. Results

3.1. Gelatin or CLP particle synthesis and influence of parameter variation

Gelatin or CLP-poly(glutamic acid)-based NPs are synthesized *via* an *in situ* polymerization of glutamic acid anhydride initiated by the amino groups present in gelatin and CLP, respectively. Thus, gelatin or CLP serve simultaneously as a macromolecular polymerization template and initiator. First, *(S)*Glu(OBzl)-NCA was obtained in a mild reaction procedure based on a protocol by *Laconde* et al. [53] To gently deprotect the acid function of PGA, a modified approach of *Conejos-Sánchez* et al. was applied [54]. Crosslinking of the resulting particles is carried out using EDEA. Finally, the particles are reacted with CDDP to form metal-polymer complexes.

3.1.1. Preparation of (S)Glu(OBzl)-NCA

Tert-butyloxycarbonyl (Boc)- and benzoyl-protected (*S*)-glutamic acid was reacted with T3P® in the presence of pyridine at room temperature (Fig. 1A). After purification by recrystallization, colorless crystals were collected in a yield of 71 %. NMR data match literature values. The corresponding spectra are attached in the supplementary information (SI, Fig. S2).

3.1.2. Preparation and characterization of CDDP-loaded Gel-PGA or CLP-PGA NPs

Polymerization of (*S*)Glu(OBzl)-NCA was started *in situ* by the amino groups of gelatin or CLP leading to nanoparticle formation (Fig. 1B). The initial gelatin or CLP solution was transparent and became opalescent upon the slow addition of (*S*)Glu(OBzl)-NCA, indicating the formation of nanoparticles. The ratio of gelatin to anhydride, the amount of the solvents as well as the reaction time affect particle size, with longer reaction times leading to larger particles. Cooling of the reaction mixture during synthesis is beneficial to obtain narrow size distributions. Additionally, anhydride purity is crucial for achieving small diameters and a narrow distribution as minimal impurities lead to aggregation. Reaction conditions and obtained particle sizes are summarized in Table S1 (SI). For all further experiments, gelatin-based NPs, were synthesized according to the optimized procedure, using 350 mg gelatin in 50 ml water and 100 mg anhydride in 4 ml DMF. For CLP-based NPs the amount of anhydride was adjusted to 85 mg in 4 ml DMF. Subsequently, the acid moieties in the PGA block were deprotected by addition of sodium hydroxide. IR spectra of protected particles display a distinctive IR peak at around 700 cm^{-1} associated with OBzl-group (out-of-plane bending vibrations of C-H bonds in aromatic rings), which is significantly reduced in the deprotected product (Fig. S4 in SI) [56,57]. Next, NPs were crosslinked using EDC/EDEA to increase stability following a protocol described by *Ding* et al. [33] After crosslinking, particles exhibited a more narrow size distribution in DLS with well-defined boundaries visible in TEM images (Fig. 3C, F). Furthermore, CLP-based particles have smaller hydrodynamic diameters at each reaction step compared to the gelatin-based NPs (Table 1). Finally, CDDP was loaded into deprotected gelatin and CLP particles using a ratio of 2:1 of CDDP to carboxy groups, free CDDP was removed by dialysis. Notably, CLP-based NPs exhibited a significantly higher platinum (Pt) content,

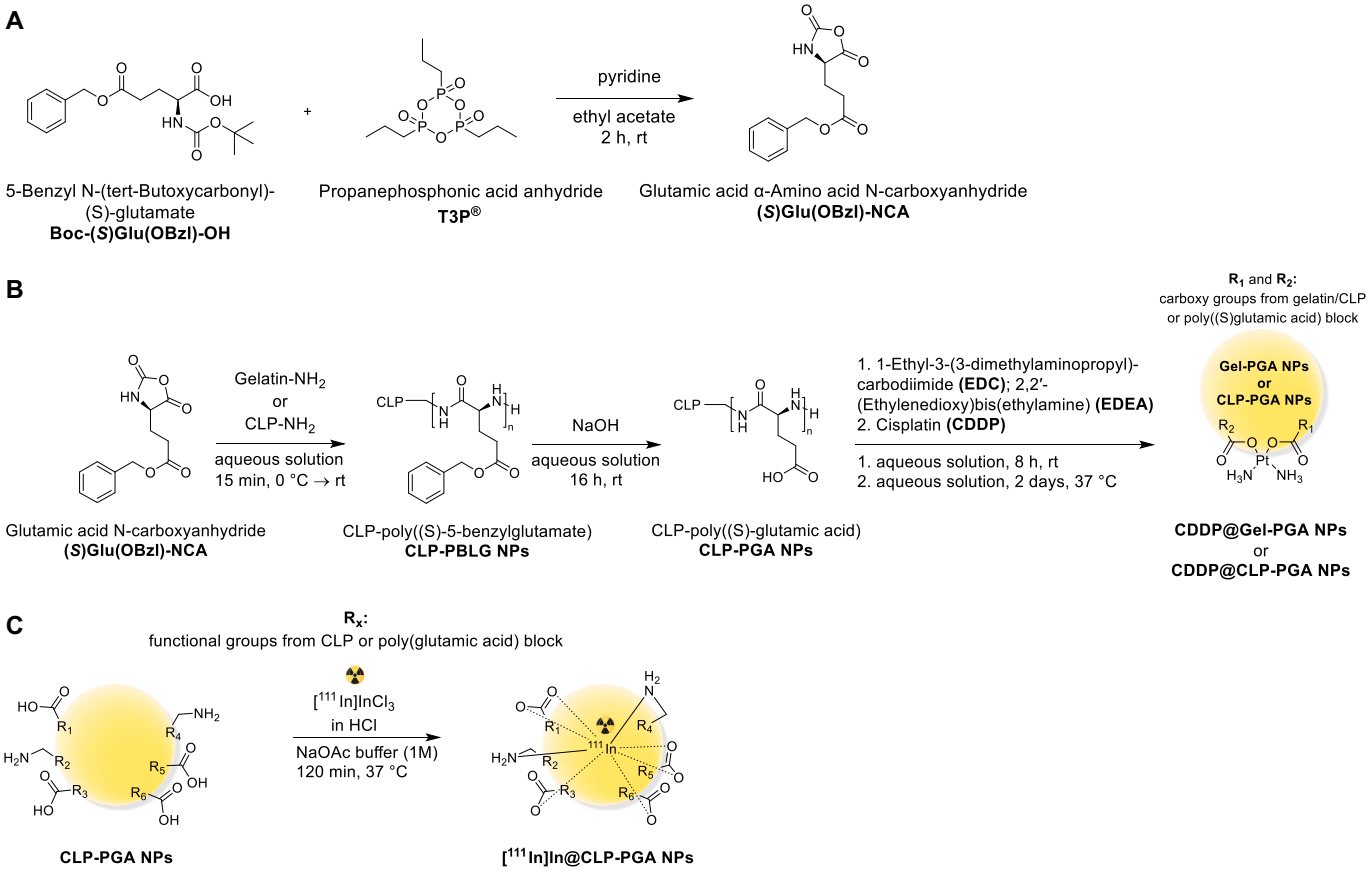

Fig. 1. A) Reaction scheme for synthesis of (*S*)Glu(OBzl)-NCA. B) Schematic representation of the synthesis process for CDDP-loaded NPs. C) Reaction scheme for NP radiolabeling.

Table 1
Characteristics of gelatin- and CLP-based NPs after each reaction step. d_H: hydrodynamic diameter, PDI: polydispersity index, d_{TEM}: diameter derived by TEM of dried particles.

Reaction step	d_H / PDI	d_{TEM}	Zeta	d_H / PDI	d_{TEM}	Zeta
	Gelatin-based NPs			CLP-based NPs		
Polymerization	258 nm / 0.253	175 ± 24 nm	−14.1 mV	296 nm / 0.251	172 ± 26 nm	9.6 mV
Deprotection	281 nm / 0.168	144 ± 18 nm	−24.1 mV	256 nm / 0.122	124 ± 23 nm	−18.4 mV
Crosslinking	241 nm / 0.177	81 ± 16 nm	−19.5 mV	223 nm / 0.137	125 ± 24 nm	−10.4 mV
CDDP complexation	191 nm / 0.219	91 ± 15 nm	−0.8 mV	155 nm / 0.125	93 ± 22 nm	21.7 mV
Pt content	0.025 mg Pt/mg NPs			0.076 mg Pt/mg NPs		

with 76 μg of Pt per mg of NPs, compared to only 25 μg of Pt per mg of NPs in the gelatin-based formulation. In addition, this approach allows for the incorporation of other platinum-based chemotherapeutics, such as oxalato(trans-l-1,2-cyclohexanediamine)platinum(II) (oxPt) (see Table S2, SI). Surface charge, size distribution and morphology were assessed for each particle system and reaction step using electrophoretic and dynamic light scattering, and TEM, respectively

For each reaction step, a significant change of the surface charge is observed, in line with earlier results for similar systems (Fig. 2A) [32]. As the surface charge is dependent on the dissociation and protonation of carboxy and amino groups, we studied the effect of pH value on surface charge by adding sodium hydroxide (0.1 M) or hydrochloric acid (0.1 M) to a dispersion of polymerized Gel-PBLG NPs. Surface potential measurements reveal a linear dependence of the surface charge on the pH of the solution (Fig. 2C). Accordingly, the surface charge after each reaction step changes with the pH obtained or used for each reaction step (Fig. 2B).

As TEM images were obtained of dried particles, diameters are considerably smaller compared to the hydrodynamic diameter but do confirm narrow size distributions (SI, Fig. S3). TEM images show that deprotection does not affect particle structure and the next crosslinking step leads to formation of smaller particles with a well-defined spherical morphology (Fig. 3). After CDDP loading, NPs appear darker with a clear edge delineation due to a higher electron density (Fig. 3D). CLP-based NPs appear smaller in diameter compared to gelatin-based NPs (Fig. 3G, H).

Overall, CLP-based NPs exhibit a narrower size distribution and smaller hydrodynamic diameters in comparison to gelatin-based NPs (Fig. 3K). CDDP complexation leads to a further reduction in particle diameters without formation of aggregates.

3.2. In vitro drug release and anti-tumoral effect

Cell viability assays with CT26 cells were performed for 48 h and 72 h incubation with free CDDP, CDDP-loaded particles and non-loaded (empty) control particles (Fig. 4A, B). The cytotoxicity of CDDP-loaded NPs is lower than that of free CDDP at the tested concentrations, which can be contributed to the slower CDDP release from the spheres. Notably, no significant effect on cell viability was observed with the empty NPs. Drug release studies conducted in fetal bovine serum (FBS) over a seven-day period revealed an initial burst release of 37 % within the first 8 h. The release profile gradually plateaued, reaching a maximum of 52 % by day seven (Fig. 4C).

3.3. Radiolabeling and in vivo biodistribution studies

3.3.1. Radiolabeling

The radionuclide indium-111, in its trivalent metal cation form ($[^{111}In]In^{3+}$) frequently employed in SPECT imaging, was used to label crosslinked, but unloaded CLP-PGA NPs (Fig. 1C). Unbound $[^{111}In]In^{3+}$ was removed *via* size exclusion chromatography (SEC), resulting in a specific activity of 5 MBq of $[^{111}In]In^{3+}$ per mg of NPs and a radiochemical purity of 90 % (Fig. S5 in SI). The surface charge increases from −10.4 mV to −9.4 mV, suggesting $[^{111}In]In^{3+}$ complexation by carboxylic acid groups, while the hydrodynamic diameter increased from 223 nm to 287 nm (Table S3 in SI). Notably, introduction of commonly employed functional chelator 2,2′,2″,2‴-(1,4,7,10-tetraazacyclododecane-1,4,7,10-tetrayl)tetraacetic acid (DOTA) did not increase radiochemical yield nor improve stability of labeled NPs (data not shown).

3.3.2. In vivo biodistribution

The biodistribution of ^{111}In-labeled CLP-based NPs was assessed in healthy mice ($n = 2$) using longitudinal SPECT/CT imaging (Fig. 5). Directly after IP injection, the scans reveal rapid signal distribution within the abdominal cavity, with notable adherence to the bowel tissue. Within the first 4 h, particles rapidly redistribute within the peritoneal cavity with changing areas of accumulation, which are difficult to link to CT-based anatomical structures. About 10 % of the injected activity (%ID) is cleared to the urine within the first 90 min. Furthermore, activity accumulation is observed at the hemisphere close to the diaphragm and above the liver. The next day, about 80 %ID remains in the entire animal followed by continuous clearance to 62 %ID on day seven (Fig. 5C). SPECT imaging reveals a redistribution of activity over several days within the abdominal cavity showing a gradual uptake inside the liver and spleen, which can be clearly recognized on day seven. Activity in the spleen reaches about 6 %ID after 4 h with a plateau value of 4 %ID after 7 days. However, at early timepoints, due to the limited resolution of SPECT imaging, it is impossible to distinguish between particle adherence to the outside of the spleen and uptake within the organ. Liver uptake proceeds exponentially for 42 h with the highest value reaching 11 %ID. At the following time points, activity accumulation remains

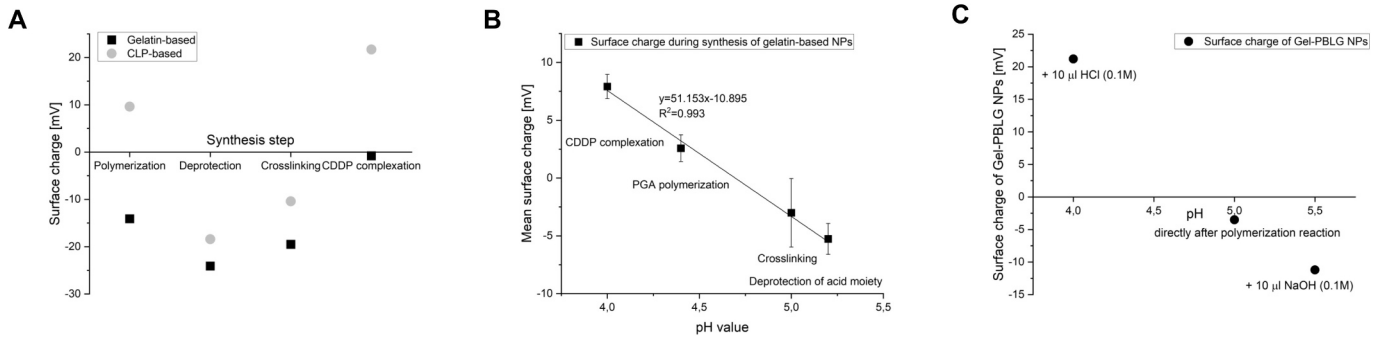

Fig. 2. Investigation on surface charge. A) Surface charge in gelatin- and CLP-based NPs depending on reaction step. B) Overview of surface charge in gelatin-based NPs as a function of pH according to reaction step ($n = 2$). C) Dependency of surface charge on pH value of Gel-PBLG-NP dispersion.

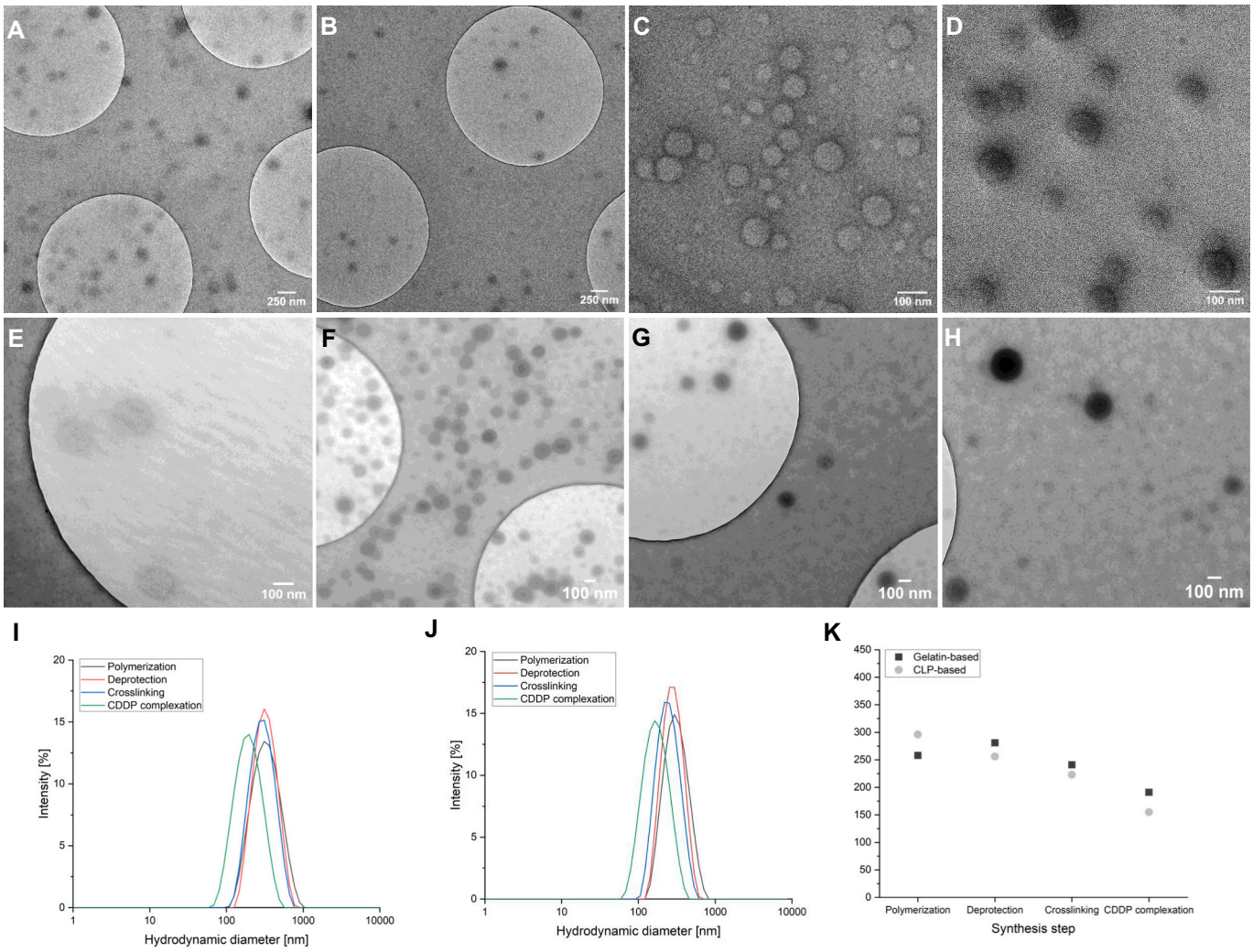

Fig. 3. TEM images of gelatin-based NPs after A) polymerization, B) deprotection, C) crosslinking D) CDDP-loading. TEM images of CLP-based NPs after E) polymerization, F) deprotection and crosslinking. TEM images of CLP-based NPs after CDDP-loading: G) overview image, H) magnified to visualize single particles. I) Hydrodynamic diameters of gelatin-based NPs in dependence of synthesis step. J) Hydrodynamic diameters of CLP-based NPs in dependence of synthesis step. K) Comparison of hydrodynamic diameters in gelatin- and CLP-based NPs in dependence of reaction step.

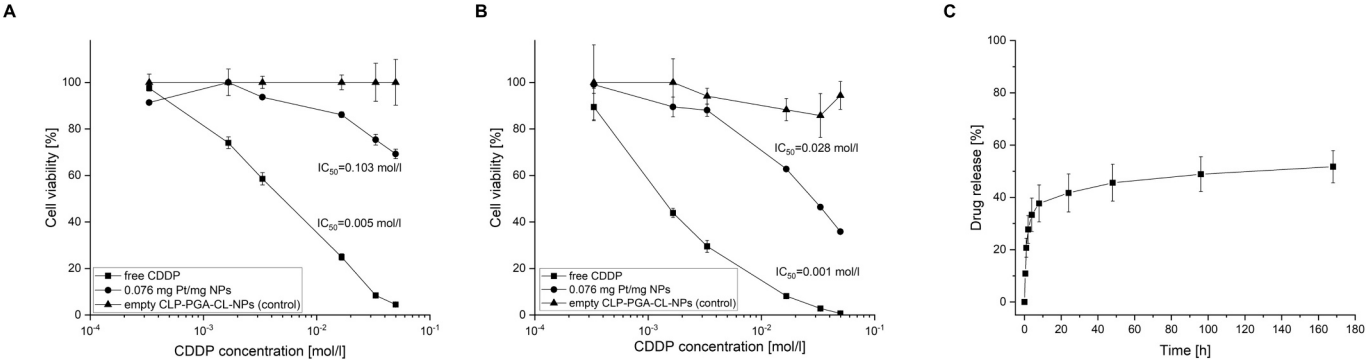

Fig. 4. Cell viability assays of CT-26 colorectal cancer cells ($n = 3$) after A) 48 h and B) 72 h incubation time of CLP-based NPs. C) Drug release of platinum in FBS over seven days.

consistent until reaching 10 %ID on day seven (Fig. 5C). The activity found in the abdominal cavity compared to the entire animal remains from day two almost constant with a ratio of 65 %. In contrast, the activity in the liver and spleen relative to the remaining abdominal space increases during the first two days, stabilizing thereafter by day seven at a constant ratio of 25 % and 11 %, respectively (Fig. 5D). Furthermore, within the first 4 h, activity is detected in the thymus region, which remains constant from day two to seven. In detail, activity is observed in the parasternal LNs indicating uptake and clearance *via* the lymphatic system. Additionally, the mediastinal LNs and also the cisterna chyli can

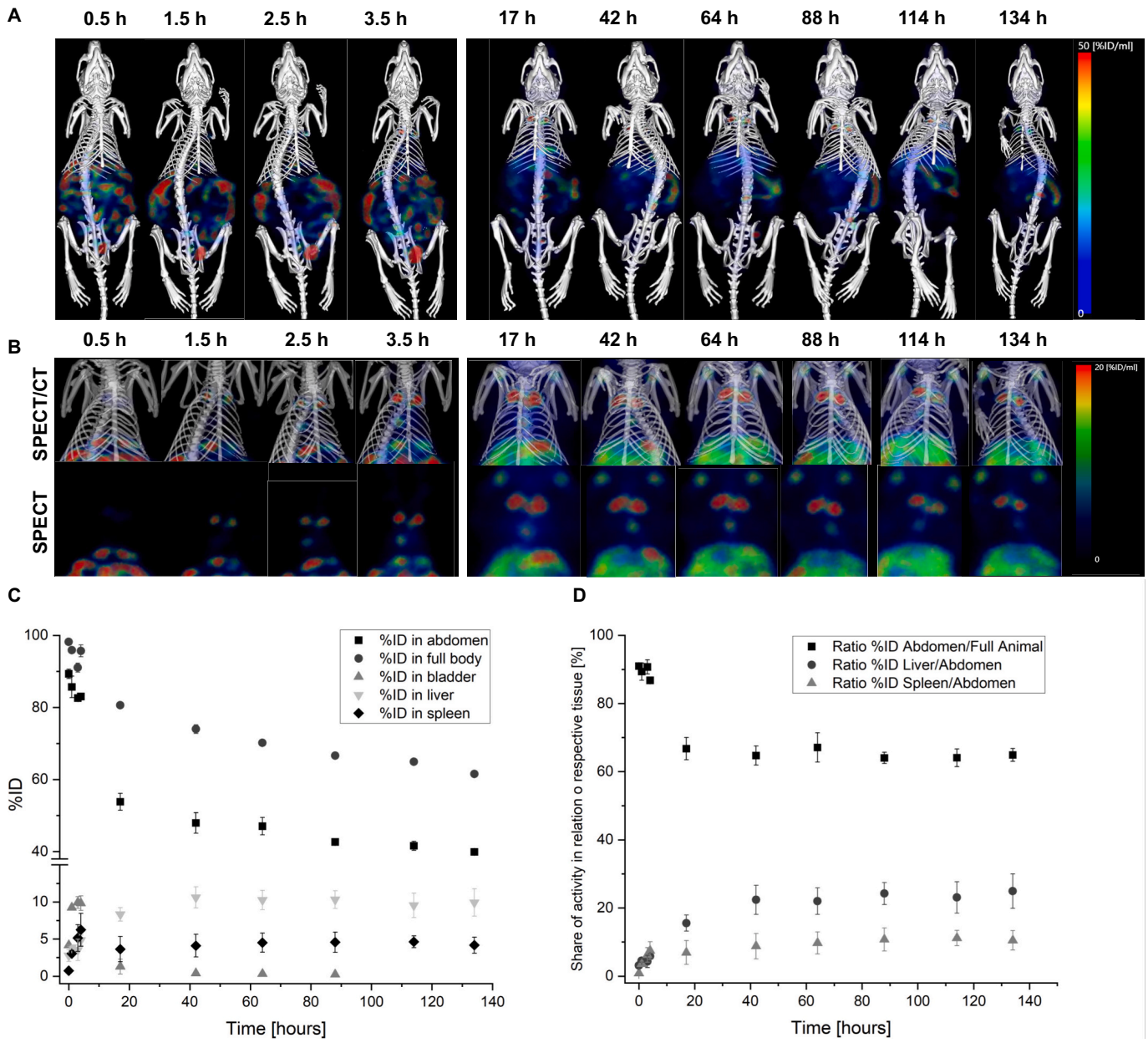

Fig. 5. SPECT/CT images of one mouse over the course of A) seven days (representative). B) SPECT images of the same mouse with window adjusted to activity levels observed in LNs (20 %ID/ml). For clarity, the same scan is displayed with and without overlay of the corresponding CT image to allow a better view of the LNs. C) SPECT evaluation: %ID of full body, abdomen, bladder, liver and spleen (n = 2). D) SPECT evaluation: Ratio of activity found in abdomen compared to whole body, liver to abdomen and spleen to abdomen (n = 2).

be identified with SPECT imaging.

Biodistribution studies performed after day seven are in line with SPECT data, with the highest uptake of activity in the spleen (121 %ID/g), followed by the kidney with 34 %ID/g. All abdominal organs are in the range of 30 %ID/g, see Figs. 6 and S6 in SI. The mesentery also demonstrated notable uptake with 24 %ID/g, while the peritoneum of healthy mice showed only an uptake of 6 %ID/g. For further localization of NPs, tissue specimens were examined with autoradiography and correlated with microscopy images (Fig. 7A). Here, autoradiography measurements show nanoparticle uptake inside liver and spleen, but also partly within the pancreas and ovaries (Fig. 7C, Table S4 in SI), while nanoparticles seem to adhere to the outside of other abdominal organs such as the colon (Fig. 7B).

4. Discussion

Treatment of patients diagnosed with PC is currently limited to palliative care. Current treatment options comprise cytoreductive surgery often followed by HIPEC or PIPEC procedures and systemic chemotherapy. However, as peritoneal metastases seed in the peritoneum, are often poorly vascularized and not (yet) connected to the systemic vascular system, systemic chemotherapy typically fails to reach therapeutically relevant drug concentrations. Moreover, tumor cells further disseminate *via* the lymphatic system, which is another source of recurrence and systemic spread. IP drug delivery has been recognized as viable option for additional treatment as higher and more local drug exposure can be achieved compared to systemic chemotherapy. As clearance of IP delivered DDSs occurs *via* the lymphatic system, reminiscent micrometastases in adjacent LNs may also receive a higher drug exposure. IP retention, distribution but also clearance pathways depend

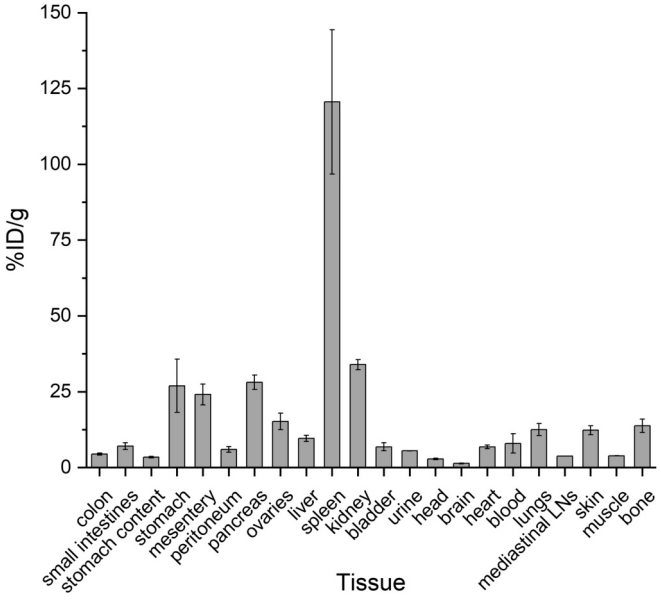

Fig. 6. Biodistribution of ^{111}In@CLP-PGA-NPs by gamma counter (n = 2).

strongly on the DDS, with size and surface charge being the most important parameters, among others [58–60]. Platinum-based drugs such as CDDP or oxPt present the most important cytostatics for treatment of PC with colorectal and gynecological cancers as primary tumor. Consequently, development of adequate DDSs providing a high payload of platinum in particles with adaptable surface charge and size is an active field of research.

In this study, we synthesized nanoparticles with diameters from 155 to 296 nm based on gelatin or CLP and PGA, providing a high load of CDDP. Our synthesis route is similar to the procedure first proposed by *Zhang* et al. to synthesize gelatin-PAA nanoparticles, which were subsequently used for loading with CDDP [31–34]. In our case, PAA was substituted for PGA due to its favorable biocompatibility and biodegradation properties. The polymerization and ring opening reaction of benzoyl-protected glutamic acid is initiated *in situ* by amino groups present in gelatin or CLP. The *in situ* polymerization of (*S*)Glu(OBzl)-NCA induced by gelatin or CLP led to nanoparticle formation in the diameter range of 100 to 200 nm. Particle diameter can be controlled by choosing different ratios of gelatin to anhydride, amount of solvents as well as reaction time. The NPs are formed by micellization, which in turn is induced by conjugation between PBLG and gelatin or CLP respectively, forming a core-shell structured particle with insoluble interpolymer complexes of PBLG and Gel/CLP as the core and soluble Gel/CLP as the shell. Hydrophilic amino-, carboxy- and hydroxyl groups in

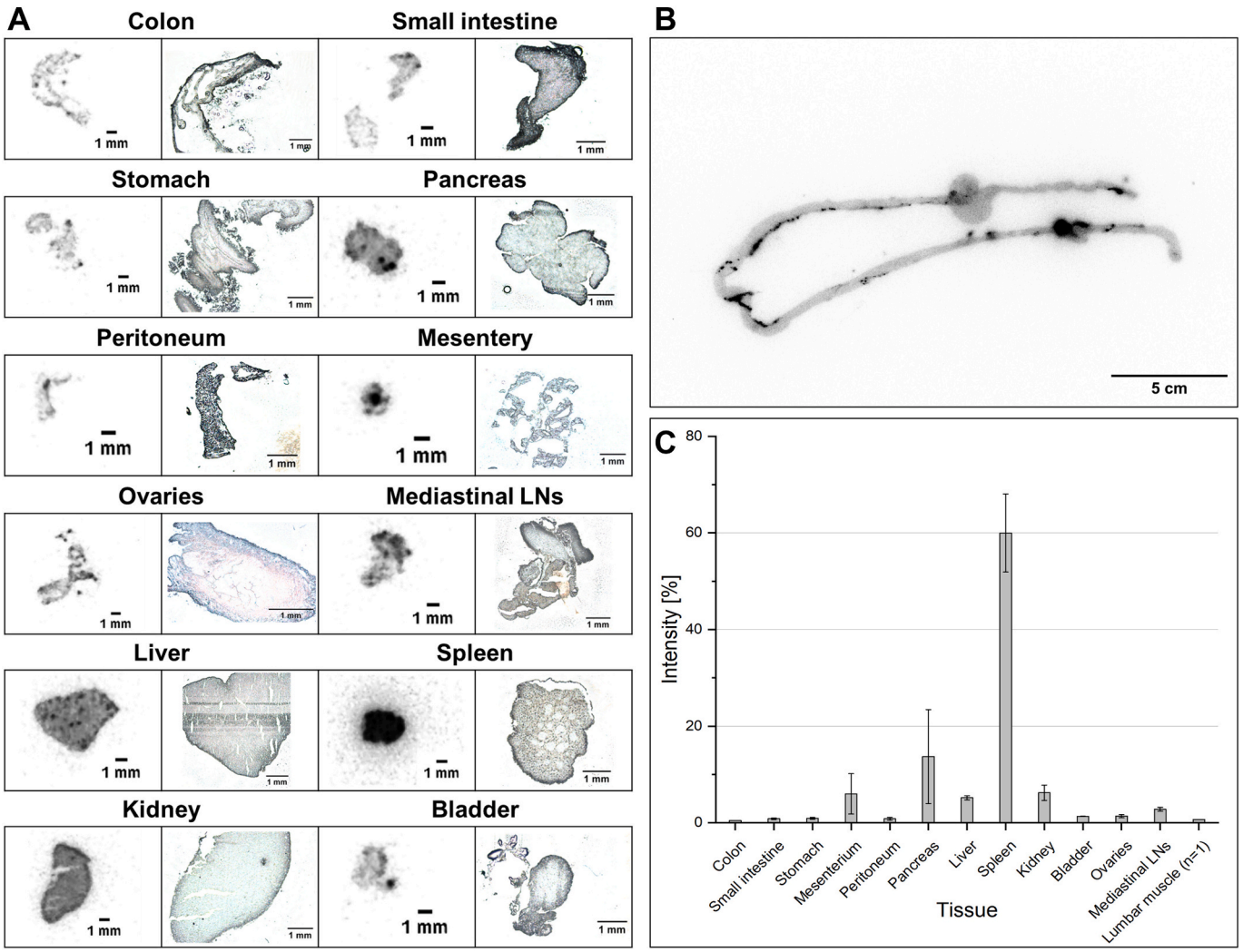

Fig. 7. A) Autoradiography and corresponding light microscope images of explanted tissues of one mouse (representative). Dark spots in autoradiography correspond to activity accumulation. B) Autoradiography image of whole colon. C) Activity accumulation in explanted tissues by autoradiography.

gelatin or CLP ensure water solubility and electrostatic stabilization of the particles.

Deprotection of the PBLG carboxy groups is reflected by the reduction of signal intensity in the range of 700 to 750 cm^{-1} in the IR spectra, typically associated with benzyl groups. Deprotection leads to formation of PGA increasing the electrostatic interactions and hydrogen bonds with gelatin or CLP reflected further in a decrease of particle diameter.

Next, particle stability was further ensured through a selective crosslinking using EDEA in the presence of EDC, which led to decrease of the particle diameter as well as PDI. Subsequent complexation with CDDP led to well-defined particles with visible boundaries in TEM images related to the high electron density of platinum. Following CDDP loading, the surface charge of both compounds increased from −19.5 mV to −0.8 mV, for gelatin-based NPs and from −10.4 mV to 21.7 mV for CLP-based NPs. Notably, CLP-based NPs have with 76 μg of CDDP per mg of NPs a significantly higher CDDP content, compared to just 25 μg of CDDP per mg of NPs in the gelatin-based NPs. The higher CDDP loading in CLP-based NPs may be attributed to CLP's chemical structure with its higher abundance of free carboxy groups facilitating higher complexation of platinum. Furthermore, incorporation of other platinum-based drugs such as oxPt is possible with this approach.

Electrophoretic light scattering performed at different pH values showed that the surface potential of gelatin-based NPs is positive (7.9 mV) at a pH about 4 after CDDP loading and negative (−5.3 mV) upon an increase in pH above 5 indicates the surface charge switch property of NPs in response to the change of medium pH. Since type-B Gel utilized in this study has an isoelectric point (pI) between 4.8 and 5.0, we suggest the microscopic structure of Gel-PGA NPs consisting of a mainly gelatin-based shell with positively charged gelatin corresponding to ionized amino groups at pH < pI or negatively charged gelatin with ionized carboxylate groups at pH > pI, which ensures NP stability at physiological pH. The particle core presumably consists of the Gel-PGA interpolyelectrolyte complex [32]. The here employed CLP has a pI of 5.5 and shows similar pH-sensitive behavior exhibiting elevated surface charge switches between reaction steps (Table 1). TEM images provide an insight into the particles' spherical morphology. Compared to physically mixed gelatin/γ-PGA nanoparticles from literature relying solely on electrostatic interaction between gelatin and pre-formed γ-PGA, our approach affords monodisperse particles with narrow size distribution (PDI of 0.1–0.2 compared to 0.4–0.6 in literature with higher PDI in drug-loaded particles) [41]. SEM images in this study showcased very strong adherence of the particles among themselves resulting in an almost gel-like structure presumed by the authors as a result of interaction between gelatin, their drug load and γ-PGA in contrast to our distinct individual spheres. This observation indicates the superior stability of our approach based on a covalently bound copolymer structure and the formation of platinum-carboxylic acid group metal complexes. Importantly, our synthesis route omits any external and potentially toxic initiator and uses only biocompatible and biodegradable building blocks. Furthermore, the employed CLP is produced by a recombinant protein manufacturing process, providing a vegan protein source with an end product having well-defined chemical properties such as a consistent amino acid sequence, monodisperse molecular weight, pharmaceutical grade purity and production reproducibility. Animal-sourced materials can be linked to undesired immunological responses, pathogens, inconsistent quality and may require more stringent regulatory control. In a clinical setting, Vecollan®-based systems may be advantageous from a regulatory perspective. Moreover, next to Vecollan®, the choice of *in situ* chemically formed α-PGA compared to bacterially produced γ-PGA for copolymer synthesis provides additional benefits. Our approach allows forming biomimetic copolymers *in situ* while the use of γ-PGA for nanoparticle synthesis is typically based on physical mixing of γ-PGA with a matrix polymer relying on electrostatic interaction [41]. One important point is the cost-intensive bacterial production. Compared to commercially available γ-PGA, the use of Boc-(*L*)Glu(OBzl)-OH educt is considerably more economical at an around 10,000-times lower cost affording (*S*)Glu(OBzl)-NCA in a scalable synthesis under mild reaction conditions. The chemical synthesis route also ensures production of low molecular weight PGA during polymerization while bacterial fermentation typically leads to high molecular weight γ-PGA in the range of 100,000 to 1,000,000 g/mol [61,62]. Also, high fluctuation of molecular weight between batches of γ-PGA is common. Firstly, this fluctuation hinders particle formation and results in polydisperse particles. Secondly, a key property for drug delivery applications is molecular weight. Thus, the polymer molecular weight has to be chosen to be high enough for prolonged residence time, and low enough to provide the proper sustained release profile during biodegradation. This molecular weight range has been determined to be around 30,000–50,000 g/mol [62–64]. Therefore, approaches for control of molecular weight of PGA are of fundamental importance for commercial development. Finally, the higher hydrophilic to hydrophobic volume ratio and reduced steric hindrance of the carboxylic acid group in α-PGA compared to γ-PGA has been shown to lead to controlled self-assembly and micellization without aggregation as well as increased drug incorporation [65].

As CLP-based NPs have a higher drug load and are more defined in structure and diameter all further studies proceeded with CLP-based particles. The toxicity of empty and CDDP loaded CLP-NPs was studied in cell viability assays compared to free drug. Empty NPs did not show any toxicity, indicating their biocompatibility. The IC_{50} for free CDDP is in the lower molar range. The IC_{50} for CDDP-loaded NPs decreased with incubation time indicating a slow but steady release. This was reinforced by drug release studies in FBS, which demonstrated an initial burst release of 37 % within 8 h, stabilizing in a gradual release pattern reaching 52 % after seven days. Most likely, the release yields not CDDP but the active metabolite cis-diammineaquachloroplatinum (II), which also forms after protein binding of CDDP [66]. The release profile is thus suitable for the intended application of IP drug delivery, where a sustained release profile is required.

As distribution within the peritoneal cavity, as well as retention and clearance pathways are essential for future optimization of the DDSs, we employed consecutive SPECT/CT studies over one week after IP injection to follow the *in vivo* behavior of CLP-PGA-CL-NPs. To this aim, particles were radiolabeled using [^{111}In]$InCl_3$. With a half-life of 2.8 days, we could track their biodistribution and clearance over seven days [67]. The high density of carboxyl and amino groups present at the nanoparticle surface facilitated the formation of strong coordination bonds with [^{111}In]In^{3+} without the need to introduce additional chelators such as DOTA moieties, as previously reported in the literature [68–70]. DLS data revealed an increase of the mean hydrodynamic particle diameter and a slight broadening of the size distribution by 60 nm, most like due to some [^{111}In]In^{3+}-induced crosslinking of individual particles. Radiolabeling barely affected surface charge with an increase from −10.4 mV before labeling to −9.8 mV after labeling.

After IP injection, SPECT analysis revealed an initial renal clearance of about 10 %ID to the bladder, of either [^{111}In]In^{3+} after initial release or small compounds after transchelation [71]. At later time points, no renal clearance was observed. Our SPECT measurements are in line with earlier observations regarding particle clearance from the IP cavity [72–75]. Particles with diameters above 20 nm are primarily cleared *via* the lymphatic system. The predominant route is the parasternal lymphatic pathway, where particles enter through ventral, diaphragmatic stomata which empty into lymphatic vessels parallel to the internal thoracic artery and finally flow to the parasternal LNs and then mediastinal LNs, clearly recognizable on SPECT images 4 h post-injection and all later timepoints. Finally, they enter into the right or thoracic lymphatic vessels with subsequent vascular recirculation [73,74,76,77]. Secondly, particles taken up *via* other diaphragmatic stomata flow through lymphatic vessels along the posterolateral aspect of the thoracic cavity, also draining into the mediastinal LNs. This pathway is therefore also known as the "thoracic cavity lymphatic" route. The third route involves visceral abdominal lymphatics that drain

into the cisterna chyli and later into the thoracic ducts. Uptake in visceral LNs and the cisterna chyli can be identified on most SPECT images as well. Imaging indicates that particles are redistributed *via* the lymphatic system, recirculated, and ultimately taken up by the liver and spleen—key clearance organs of the mononuclear phagocyte system (MPS). SPECT imaging showed that by day seven, approximately 40 %ID remained overall in the peritoneal cavity, with 14 % having accumulated in the liver and spleen. Taking these two sites into consideration, a total activity of 26 %ID remained in the abdominal cavity after seven days. As the limited spatial resolution of SPECT imaging does not allow distinguishing between NP uptake and adsorption to outer tissue boundaries, autoradiography images were acquired for tissue slices. While liver and spleen sections show homogeneous uptake of radiolabeled particles, NPs are mainly sticking to the outer tissue layer of other abdominal organs such as colon, mesothelium, mesentery, peritoneum, kidney, *etc.* The mesentery, which is one of the prime locations of IP metastasis, showed notable uptake, accumulating approximately 24 %ID/g. Interestingly, the pancreas and ovaries showed mixed results with NP accumulation on the organ's surface as well as uptake within the organs.

In summary, SPECT imaging, autoradiography as well as biodistribution data demonstrate that NPs are cleared through known lymphatic pathways, which feed into the venous system. Subsequent recirculation, alongside phagocytosis leads to clearance by the MPS with uptake in liver and spleen. Previous studies showed that particle size and surface charge are the main factors determining clearance pathways, retention time within the IP cavity, potential adhesion near injection site but also tumor uptake. With respect to size, contradictory requirements exist as larger particles (*i.e.* diameter above 2–5 μm) show prolonged retention as the stomata have a size cut-off in that range, while small particles seem to show improved tumor uptake [58,59,78,79]. As our CLP-based NPs may be tuned in size from nano- to microparticles as well as in surface charge by possible surface modification with charged groups, they are an ideal platform to further study the most suitable properties for IP drug delivery. Furthermore, they can be loaded with other platinum-based drugs such as oxPt or carboplatin, next to CDDP addressing different tumor entities. SPECT imaging, combined with autoradiography, is a perfect tool to track the pharmacokinetics of particle clearance as well as their spatial redistribution in the intraperitoneal cavity.

5. Conclusion

In this study, CDDP was loaded into Gel-PGA or CLP-PGA NPs through the interaction between the platinum of CDDP and the carboxyl groups of the NPs with high drug loading and stability. The obtained NPs have a spherical structure with an average diameter of about 150 nm as measured by DLS. We would like to emphasize that purity of the synthesized (*S*)Glu(OBzl)-NCA is key to obtain NPs with a well-defined diameter and narrow size distribution. Furthermore, gelatin-based NPs require extensive purification of the used gelatin with different NP diameters obtained for different gelatin lots. The latter highlights the advantage to use CLP-based particles that ensure well-controlled NP synthesis, which is of importance for any future clinical translation from a regulatory perspective. The CDDP-loaded NPs demonstrated extended-release characteristics, suggesting their potential for sustained drug release. Subsequently, longitudinal SPECT/CT imaging using radiolabeled but unloaded NPs was used to assess kinetic and biodistribution of the DDS in healthy mice. After IP injection, particles are cleared *via* the lymphatic system into the venous system. Subsequently, particles are recirculated with final uptake in liver and spleen. After seven days, a significant amount is still present in other abdominal organs such as pancreas and ovaries, in addition to particles adhering to the surface of abdominal tissues. These results show, that our NPs do not aggregate significantly upon IP injection but are distributed and cleared mostly as individual particles, which is a prerequisite for future therapeutic application. Overall, the results support the use of CLP-PGA NPs as a promising drug carrier for passive distribution and controlled release, with potential for localized treatments in IP drug delivery.

CRediT authorship contribution statement

Xenia Kovalyk: Writing – review & editing, Writing – original draft, Visualization, Methodology, Investigation, Formal analysis, Data curation, Conceptualization. **Sven Saniternik:** Investigation, Formal analysis. **Larissa-M. Hamacher:** Investigation. **Ben Lasse Mink:** Investigation. **Sven Thoröe-Boveleth:** Resources. **Patricia Bach:** Resources. **Thomas Endres:** Resources. **Maria Montero-Mirabet:** Resources. **Annette M. Schmidt:** Writing – review & editing, Supervision, Resources. **Holger Grüll:** Writing – review & editing, Supervision, Funding acquisition, Conceptualization.

Funding sources

This research did not receive any specific grant from funding agencies in the public, commercial, or not-for-profit sectors.

Declaration of competing interest

The authors declare the following financial interests/personal relationships which may be considered as potential competing interests: Xenia Kovalyk reports financial support and drugs were provided by Evonik Foundation. Thomas Endres reports a relationship with Evonik Operations GmbH that includes: employment. Maria Montero-Mirabet reports a relationship with Evonik Operations GmbH that includes: employment. If there are other authors, they declare that they have no known competing financial interests or personal relationships that could have appeared to influence the work reported in this paper.

Acknowledgements

The authors thank the Evonik Foundation for their scholarship supporting Xenia Kovalyk. We thankfully acknowledge Fatma Simsek and Tom Schneider for their contributions to our studies.

Appendix A. Supplementary data

Supplementary data to this article can be found online at https://doi.org/10.1016/j.bioadv.2025.214601.

Data availability

Data will be made available on request.

References

[1] A. Rijken, R.J. Lurvink, M.D. Luyer, G.A. Nieuwenhuijzen, F.N. van Erning, J. W. van Sandick, et al., The burden of peritoneal metastases from gastric cancer: a systematic review on the incidence, risk factors and survival, J. Clin. Med. 10 (2021) 4882.
[2] I. Thomassen, Y.R. van Gestel, B. van Ramshorst, M.D. Luyer, K. Bosscha, S. W. Nienhuijs, et al., Peritoneal carcinomatosis of gastric origin: a population-based study on incidence, survival and risk factors, Int. J. Cancer 134 (2014) 622–628.
[3] L. Burg, M. Timmermans, A.A.M. Van Der, D. Boll, K. Rovers, I. de Hingh, et al., Incidence and predictors of peritoneal metastases of gynecological origin: a population-based study in the Netherlands, J. Gynecol. Oncol. 31 (2020) e58.
[4] D. Cortés-Guiral, M. Hübner, M. Alyami, A. Bhatt, W. Ceelen, O. Glehen, et al., Primary and metastatic peritoneal surface malignancies, Nat. Rev. Dis. Primers. 7 (2021) 1–23, https://doi.org/10.1038/s41572-021-00326-6.
[5] A. Brind'Amour, M. Webb, M. Parapini, L. Sidéris, M. Segedi, S.W. Chung, et al., The role of intraperitoneal chemotherapy in the surgical management of pancreatic ductal adenocarcinoma: a systematic review, Clin. Exp. Metastasis 38 (2021) 187–196.
[6] K. De Clercq, F. Xie, O. De Wever, B. Descamps, A. Hoorens, A. Vermeulen, et al., Preclinical evaluation of local prolonged release of paclitaxel from gelatin microspheres for the prevention of recurrence of peritoneal carcinomatosis in

advanced ovarian cancer, Sci. Rep. 9 (2019) 14881, https://doi.org/10.1038/s41598-019-51419-y.
[7] W. Ceelen, L. Sandra, L.V. De Sande, M. Graversen, M.B. Mortensen, A. Vermeulen, et al., Phase I study of intraperitoneal aerosolized nanoparticle albumin based paclitaxel (NAB-PTX) for unresectable peritoneal metastases, eBioMedicine 82 (2022) 104151, https://doi.org/10.1016/j.ebiom.2022.104151.
[8] S.K. Williamson, G.A. Johnson, H.A. Maulhardt, K.M. Moore, D.S. McMeekin, T. K. Schulz, et al., A phase I study of intraperitoneal nanoparticulate paclitaxel (Nanotax®) in patients with peritoneal malignancies, Cancer Chemother. Pharmacol. 75 (2015) 1075–1087.
[9] M.C. Cristea, P. Frankel, T. Synold, S. Rivkin, D. Lim, V. Chung, et al., A phase I trial of intraperitoneal nab-paclitaxel in the treatment of advanced malignancies primarily confined to the peritoneal cavity, Cancer Chemother. Pharmacol. 83 (2019) 589–598.
[10] N. Lang, A. Diciola, I. Labidi-Galy, F. Ris, M. Di Marco, N. Mach, et al., Nab-PIPAC: a phase IB study protocol of intraperitoneal cisplatin and nab-paclitaxel administered by pressurised intraperitoneal aerosol chemotherapy (PIPAC) in the treatment of advanced malignancies confined to the peritoneal cavity, BMJ Open 13 (2023) e067691.
[11] M. Choi, M.M. Harper, P.K. Pandalai, S.R. Abdel-Misih, R.A. Patel, C.S. Ellis, et al., A multicenter phase 1 trial evaluating nanoliposomal irinotecan for heated intraperitoneal chemotherapy combined with cytoreductive surgery for patients with peritoneal surface disease, Ann. Surg. Oncol. 30 (2023) 804–813.
[12] S. Alavi, A. Haeri, I. Mahlooji, S. Dadashzadeh, Tuning the physicochemical characteristics of particle-based carriers for intraperitoneal local chemotherapy, Pharm. Res. 37 (2020) 119, https://doi.org/10.1007/s11095-020-02818-8.
[13] M. Tsai, Z. Lu, J. Wang, T.-K. Yeh, M.G. Wientjes, J.L.-S. Au, Effects of carrier on disposition and antitumor activity of intraperitoneal paclitaxel, Pharm. Res. 24 (2007) 1691–1701, https://doi.org/10.1007/s11095-007-9298-0.
[14] H. Qu, J. Yang, S. Li, J. Xu, X. Zhou, X. Xue, et al., Programmed-response cross-linked nanocarrier for multidrug-resistant ovarian cancer treatment, J. Control. Release 357 (2023) 274–286, https://doi.org/10.1016/j.jconrel.2023.03.031.
[15] H. Qian, K. Qian, J. Cai, Y. Yang, L. Zhu, B. Liu, Therapy for gastric cancer with peritoneal metastasis using injectable albumin hydrogel hybridized with paclitaxel-loaded red blood cell membrane nanoparticles, ACS Biomater Sci. Eng. 5 (2019) 1100–1112, https://doi.org/10.1021/acsbiomaterials.8b01557.
[16] Q. Yun, S.S. Wang, S. Xu, J.P. Yang, J. Fan, L.L. Yang, et al., Use of 5-fluorouracil loaded micelles and cisplatin in thermosensitive chitosan hydrogel as an efficient therapy against colorectal peritoneal carcinomatosis, Macromol. Biosci. 17 (2017) 1600262.
[17] T.D. Yan, F. Chu, M. Links, P.C. Kam, D. Glenn, D.L. Morris, Cytoreductive surgery and perioperative intraperitoneal chemotherapy for peritoneal carcinomatosis from colorectal carcinoma: non-mucinous tumour associated with an improved survival, Eur. J. Surg. Oncol. (EJSO) 32 (2006) 1119–1124.
[18] T.D. Yan, L. Welch, D. Black, P.H. Sugarbaker, A systematic review on the efficacy of cytoreductive surgery combined with perioperative intraperitoneal chemotherapy for diffuse malignancy peritoneal mesothelioma, Ann. Oncol. 18 (2007) 827–834.
[19] L. Ansaloni, F. Coccolini, L. Morosi, A. Ballerini, M. Ceresoli, G. Grosso, et al., Pharmacokinetics of concomitant cisplatin and paclitaxel administered by hyperthermic intraperitoneal chemotherapy to patients with peritoneal carcinomatosis from epithelial ovarian cancer, Br. J. Cancer 112 (2015) 306–312.
[20] S.L. Aronson, M. Lopez-Yurda, S.N. Koole, J.H.S. van Leeuwen, H.W.R. Schreuder, R.H.M. Hermans, et al., Cytoreductive surgery with or without hyperthermic intraperitoneal chemotherapy in patients with advanced ovarian cancer (OVHIPEC-1): final survival analysis of a randomised, controlled, phase 3 trial, Lancet Oncol. 0 (2023), https://doi.org/10.1016/S1470-2045(23)00396-0.
[21] A. Pinto, M. Pocard, Hyperthermic intraperitoneal chemotherapy with cisplatin and mitomycin C for colorectal cancer peritoneal metastases: a systematic review of the literature, Pleura Peritoneum 4 (2019) 20190006.
[22] S.M. Abuzar, E.J. Park, Y. Seo, J. Lee, S.H. Baik, S.-J. Hwang, Preparation and evaluation of intraperitoneal long-acting oxaliplatin-loaded multi-vesicular liposomal depot for colorectal cancer treatment, Pharmaceutics 12 (2020) 736.
[23] A.G.W.E. Wintjens, H. Liu, P.-P.K.H. Fransen, K. Lenaerts, G.C. van Almen, M. J. Gijbels, et al., Treating colorectal peritoneal metastases with an injectable cytostatic loaded supramolecular hydrogel in a rodent animal model, Clin. Exp. Metastasis 40 (2023) 243–253, https://doi.org/10.1007/s10585-023-10210-0.
[24] M.T. Perelló-Trias, A.J. Serrano-Muñoz, A. Rodríguez-Fernández, J.J. Segura-Sampedro, J.M. Ramis, M. Monjo, Intraperitoneal drug delivery systems for peritoneal carcinomatosis: bridging the gap between research and clinical implementation, J. Control. Release 373 (2024) 70–92, https://doi.org/10.1016/j.jconrel.2024.07.017.
[25] K. Yamashita, S. Tsunoda, S. Gunji, T. Murakami, T. Suzuki, Y. Tabata, et al., Intraperitoneal chemotherapy for peritoneal metastases using sustained release formula of cisplatin-incorporated gelatin hydrogel granules, Surg. Today 49 (2019) 785–794, https://doi.org/10.1007/s00595-019-01792-y.
[26] W.I. Sundquist, K.J. Ahmed, L.S. Hollis, S.J. Lippard, Solvolysis reactions of cis-and trans-diamminedichloroplatinum (II) in dimethyl sulfoxide. Structural characterization and DNA binding of trans-bis (ammine) chloro (DMSO) platinum (1+), Inorg. Chem. 26 (1987) 1524–1528.
[27] D. Moreno, Characterization of cisplatin cytotoxicity delivered from PLGA-systems, Eur. J. Pharm. Biopharm. 68 (2008) 503–512, https://doi.org/10.1016/j.ejpb.2007.08.006.
[28] X. Li, R. Li, X. Qian, Y. Ding, Y. Tu, R. Guo, et al., Superior antitumor efficiency of cisplatin-loaded nanoparticles by intratumoral delivery with decreased tumor metabolism rate, Eur. J. Pharm. Biopharm. 70 (2008) 726–734.
[29] N. Nishiyama, Y. Kato, Y. Sugiyama, K. Kataoka, Cisplatin-loaded polymer-metal complex micelle with time-modulated decaying property as a novel drug delivery system, Pharm. Res. 18 (2001) 1035–1041.
[30] W. Zhuang, B. Ma, G. Liu, X. Chen, Y. Wang, A fully absorbable biomimetic polymeric micelle loaded with cisplatin as drug carrier for cancer therapy, Regen. Biomater. 5 (2018) 1–8.
[31] Y. Zhang, Z. Wang, Y. Wang, J. Zhao, C. Wu, Facile preparation of pH-responsive gelatin-based core–shell polymeric nanoparticles at high concentrations via template polymerization, Polymer 48 (2007) 5639–5645, https://doi.org/10.1016/j.polymer.2007.07.046.
[32] D. Ding, Z. Zhu, Q. Liu, J. Wang, Y. Hu, X. Jiang, et al., Cisplatin-loaded gelatin-poly (acrylic acid) nanoparticles: synthesis, antitumor efficiency in vivo and penetration in tumors, Eur. J. Pharm. Biopharm. 79 (2011) 142–149.
[33] D. Ding, Z. Zhu, R. Li, X. Li, W. Wu, X. Jiang, et al., Nanospheres-incorporated implantable hydrogel as a trans-tissue drug delivery system, ACS Nano 5 (2011) 2520–2534, https://doi.org/10.1021/nn102138u.
[34] D. Ding, J. Wang, Z. Zhu, R. Li, W. Wu, B. Liu, et al., Tumor accumulation, penetration, and antitumor response of cisplatin-loaded gelatin/poly(acrylic acid) nanoparticles, ACS Appl. Mater. Interfaces 4 (2012) 1838–1846, https://doi.org/10.1021/am300138z.
[35] W. Zhang, H. Shen, Y. Li, K. Yang, P. Lei, Y. Gu, et al., Preparation of type-a gelatin/poly-γ-glutamic acid nanoparticles for enhancing the stability and bioavailability of (−)-epigallocatechin gallate, Foods 12 (2023) 1748, https://doi.org/10.3390/foods12091748.
[36] Y. Zhang, W. Song, Y. Lu, Y. Xu, C. Wang, D.-G. Yu, et al., Recent advances in poly (α-L-glutamic acid)-based nanomaterials for drug delivery, Biomolecules 12 (2022) 636, https://doi.org/10.3390/biom12050636.
[37] Z. Jiang, X. Feng, H. Zou, W. Xu, X. Zhuang, Poly(l-glutamic acid)-cisplatin nanoformulations with detachable PEGylation for prolonged circulation half-life and enhanced cell internalization, Bioact. Mater. 6 (2021) 2688–2697, https://doi.org/10.1016/j.bioactmat.2021.01.034.
[38] Y. Xiong, W. Jiang, Y. Shen, H. Li, C. Sun, A. Ouahab, et al., A poly(γ, l-glutamic acid)-citric acid based nanoconjugate for cisplatin delivery, Biomaterials 33 (2012) 7182–7193, https://doi.org/10.1016/j.biomaterials.2012.06.071.
[39] Y. Otani, Y. Tabata, Y. Ikada, Rapidly curable biological glue composed of gelatin and poly(l-glutamic acid), Biomaterials 17 (1996) 1387–1391, https://doi.org/10.1016/0142-9612(96)87279-6.
[40] Y. Otani, Y. Tabata, Y. Ikada, Effect of additives on gelation and tissue adhesion of gelatin–poly(L-glutamic acid) mixture, Biomaterials 19 (1998) 2167–2173, https://doi.org/10.1016/S0142-9612(98)00123-9.
[41] W. Zhang, H. Shen, Y. Li, K. Yang, P. Lei, Y. Gu, et al., Preparation of type-A gelatin/poly-γ-glutamic acid nanoparticles for enhancing the stability and bioavailability of (−)-epigallocatechin gallate, Foods 12 (2023) 1748, https://doi.org/10.3390/foods12091748.
[42] B. Liu, W. Huang, G. Yang, Y. An, Y. Yin, N. Wang, et al., Preparation of gelatin/poly (γ-glutamic acid) hydrogels with stimulated response by hot-pressing preassembly and radiation crosslinking, Mater. Sci. Eng. C 116 (2020) 111259, https://doi.org/10.1016/j.msec.2020.111259.
[43] C. Dou, Z. Li, Y. Luo, J. Gong, Q. Li, J. Zhang, et al., Bio-based poly (γ-glutamic acid)-gelatin double-network hydrogel with high strength for wound healing, Int. J. Biol. Macromol. 202 (2022) 438–452, https://doi.org/10.1016/j.ijbiomac.2022.01.057.
[44] Y.-C. Kuo, S.-Y. Lin, S. De, R. Rajesh, Regeneration of pancreatic cells using optimized nanoparticles and l-glutamic acid–gelatin scaffolds with controlled topography and grafted activin A/BMP4, ACS Biomater Sci. Eng. 9 (2023) 6208–6224, https://doi.org/10.1021/acsbiomaterials.3c00791.
[45] J.-J. Yang, Y.-Y. Lin, K.-H. Chao, J.-L. Wang, Gelatin–poly (γ-glutamic acid) hydrogel as a potential adhesive for repair of intervertebral disc annulus fibrosus: evaluation of cytocompatibility and degradability, Spine 46 (2021) E243, https://doi.org/10.1097/BRS.0000000000003767.
[46] C. Liang, C.-W. Wang, Assessing acute toxicity potential of persulfate ISCO treated water, Chemosphere 93 (2013) 2711–2716, https://doi.org/10.1016/j.chemosphere.2013.08.078.
[47] X. Muñoz, M.-J. Cruz, R. Orriols, C. Bravo, M. Espuga, F. Morell, Occupational asthma due to persulfate saltsa, Chest 123 (2003) 2124–2129, https://doi.org/10.1378/chest.123.6.2124.
[48] K. Aalto-Korte, S. Mäkinen-Kiljunen, Specific immunoglobulin E in patients with immediate persulfate hypersensitivity, Contact Dermatitis 49 (2003) 22–25, https://doi.org/10.1111/j.0105-1873.2003.00134.x.
[49] D. Liu, Y. Nashed-Samuel, P.V. Bondarenko, D.N. Brems, D. Ren, Interactions between therapeutic proteins and acrylic acid leachable, PDA J. Pharm. Sci. Technol. 66 (2012) 12–19, https://doi.org/10.5731/pdajpst.2012.00803.
[50] D.C. Dorman, M.L. Foster, B. Olesnevich, B. Bolon, A. Castel, M. Sokolsky-Papkov, et al., Toxicity associated with ingestion of a polyacrylic acid hydrogel dog pad, J. Vet. Diagn. Invest. 30 (2018) 708–714, https://doi.org/10.1177/1040638718782583.
[51] B. van Bochove, L. Warmink, M. Ankoné, D. Grijpma, A. Poot, Porous photo-crosslinked hybrid networks based on poly(trimethylene carbonate-*co*-ε-caprolactone) and recombinant human-like collagen, Biomater. Adv. 167 (2025) 214106, https://doi.org/10.1016/j.bioadv.2024.214106.
[52] S. Rigogliuso, S. Campora, M. Notarbartolo, G. Ghersi, Recovery of bioactive compounds from marine organisms: focus on the future perspectives for pharmacological, biomedical and regenerative medicine applications of marine collagen, Molecules 28 (2023) 1152, https://doi.org/10.3390/molecules28031152.

[53] G. Laconde, M. Amblard, J. Martinez, Synthesis of α-amino acid *N*-carboxyanhydrides, Org. Lett. 23 (2021) 6412–6416, https://doi.org/10.1021/acs.orglett.1c02224.
[54] I. Conejos-Sánchez, A. Duro-Castano, A. Birke, M. Barz, M.J. Vicent, A controlled and versatile NCA polymerization method for the synthesis of polypeptides, Polym. Chem. 4 (2013) 3182–3186, https://doi.org/10.1039/C3PY00347G.
[55] F. Gremse, M. Stärk, J. Ehling, J.R. Menzel, T. Lammers, F. Kiessling, Imalytics preclinical: interactive analysis of biomedical volume data, Theranostics 6 (2016) 328–341, https://doi.org/10.7150/thno.13624.
[56] M. Margoshes, V.A. Fassel, The infrared spectra of aromatic compounds: I. the out-of-plane C-H bending vibrations in the region 625–900 cm−1, Spectrochim. Acta 7 (1955) 14–24, https://doi.org/10.1016/0371-1951(55)80003-3.
[57] R.D. Kross, V.A. Fassel, M. Margoshes, The infrared spectra of aromatic compounds. II. Evidence concerning the interaction of π-electrons and σ-bond orbitals in CH out-of-plane bending Vibrations1, J. Am. Chem. Soc. 78 (1956) 1332–1335.
[58] G. Lee, S. Han, I. Inocencio, E. Cao, J. Hong, A.R.J. Phillips, et al., Lymphatic uptake of liposomes after intraperitoneal administration primarily occurs via the diaphragmatic lymphatics and is dependent on liposome surface properties, Mol. Pharm. 16 (2019) 4987–4999, https://doi.org/10.1021/acs.molpharmaceut.9b00855.
[59] P. Dogra, N.L. Adolphi, Z. Wang, Y.-S. Lin, K.S. Butler, P.N. Durfee, et al., Establishing the effects of mesoporous silica nanoparticle properties on in vivo disposition using imaging-based pharmacokinetics, Nat. Commun. 9 (2018) 4551, https://doi.org/10.1038/s41467-018-06730-z.
[60] S. Pan, H. Yuan, Q. Zhai, Y. Zhang, H. He, T. Yin, et al., The journey of nanoparticles in the abdominal cavity: exploring their *in vivo* fate and impact factors, J. Control. Release 376 (2024) 266–285, https://doi.org/10.1016/j.jconrel.2024.10.011.
[61] I.-L. Shih, Y.-T. Van, The production of poly-(γ-glutamic acid) from microorganisms and its various applications, Bioresour. Technol. 79 (2001) 207–225, https://doi.org/10.1016/S0960-8524(01)00074-8.
[62] I. Bajaj, R. Singhal, Poly (glutamic acid)–an emerging biopolymer of commercial interest, Bioresour. Technol. 102 (2011) 5551–5561.
[63] J.W. Singer, R. Bhatt, J. Tulinsky, K.R. Buhler, E. Heasley, P. Klein, et al., Water-soluble poly-(l-glutamic acid)–Gly-camptothecin conjugates enhance camptothecin stability and efficacy in vivo, J. Control. Release 74 (2001) 243–247, https://doi.org/10.1016/S0168-3659(01)00323-6.
[64] F. Ye, T. Ke, E.-K. Jeong, X. Wang, Y. Sun, M. Johnson, et al., Noninvasive visualization of in vivo drug delivery of poly(l-glutamic acid) using contrast-enhanced MRI, Mol. Pharm. 3 (2006) 507–515, https://doi.org/10.1021/mp060052g.
[65] Y. Guo, Y. Shen, B. Yu, L. Ding, Z. Meng, X. Wang, et al., Hydrophilic poly(glutamic acid)-based nanodrug delivery system: structural influence and antitumor efficacy, Polymers 14 (2022) 2242, https://doi.org/10.3390/polym14112242.
[66] F.F. Farris, F.G. King, R.L. Dedrick, C.L. Litterst, Physiological model for the pharmacokinetics of cis-dichlorodiammineplatinum (II)(DDP) in the tumored rat, J. Pharmacokinet. Biopharm. 13 (1985) 13–39.
[67] D. Psimadas, P. Georgoulias, V. Valotassiou, G. Loudos, Molecular nanomedicine towards cancer: 111In-labeled nanoparticles, J. Pharm. Sci. 101 (2012) 2271–2280, https://doi.org/10.1002/jps.23146.
[68] M. Krekorian, G.G.W. Sandker, K.R.G. Cortenbach, O. Tagit, N.K. van Riessen, R. Raavé, et al., Characterization of intrinsically radiolabeled poly(lactic-co-glycolic acid) nanoparticles for ex vivo autologous cell labeling and in vivo tracking, Bioconjug. Chem. 32 (2021) 1802–1811, https://doi.org/10.1021/acs.bioconjchem.1c00271.
[69] R. Cartier, L. Kaufner, B.R. Paulke, R. Wüstneck, S. Pietschmann, R. Michel, et al., Latex nanoparticles for multimodal imaging and detection *in vivo*, Nanotechnology 18 (2007) 195102, https://doi.org/10.1088/0957-4484/18/19/195102.
[70] L. Stelter, J.G. Pinkernelle, R. Michel, R. Schwartländer, N. Raschzok, M.H. Morgul, et al., Modification of aminosilanized superparamagnetic nanoparticles: feasibility of multimodal detection using 3T MRI, small animal PET, and fluorescence imaging, Mol. Imaging Biol. 12 (2010) 25–34, https://doi.org/10.1007/s11307-009-0237-9.
[71] N.M. Hijnen, A. de Vries, K. Nicolay, H. Grüll, Dual-isotope 111In/177Lu SPECT imaging as a tool in molecular imaging tracer design, Contrast Media Mol. Imaging 7 (2012) 214–222.
[72] C.-C. Chen, J.-J. Li, N.-H. Guo, D.-Y. Chang, C.-Y. Wang, J.-T. Chen, et al., Evaluation of the biological behavior of a gold nanocore-encapsulated human serum albumin nanoparticle (Au@HSANP) in a CT-26 tumor/ascites mouse model after intravenous/intraperitoneal administration, Int. J. Mol. Sci. 20 (2019) 217, https://doi.org/10.3390/ijms20010217.
[73] P.H. Simer, The passage of particulate matter from the peritoneal cavity into the lymph vessels of the diaphragm, Anat. Rec. 101 (1948) 333–351.
[74] T. Olin, T. Saldeen, The lymphatic pathways from the peritoneal cavity: a lymphangiographic study in the rat, Cancer Res. 24 (1964) 1700–1711.
[75] G. Király, J.C. Egu, Z. Hargitai, I. Kovács, I. Fábián, J. Kalmár, et al., Mesoporous aerogel microparticles injected into the abdominal cavity of mice accumulate in parathymic lymph nodes, Int. J. Mol. Sci. 22 (2021) 9756.
[76] M. Pasierbek, Functional anatomy of the mediastinal lymph nodes in rats, Lymphat. Res. Biol. 12 (2014) 157–163.
[77] A.J. Marco, M. Domingo, J. Ruberte, A. Carretero, V. Briones, L. Dominguez, Lymphatic drainage of Listeria inonocytogenes and Indian ink inoculated in the peritoneal cavity of the mouse, Lab. Anim 26 (1992) 200–205.
[78] N. Mirahmadi, M.H. Babaei, A.M. Vali, S. Dadashzadeh, Effect of liposome size on peritoneal retention and organ distribution after intraperitoneal injection in mice, Int. J. Pharm. 383 (2010) 7–13.
[79] S. Dadashzadeh, N. Mirahmadi, M.H. Babaei, A.M. Vali, Peritoneal retention of liposomes: effects of lipid composition, PEG coating and liposome charge, J. Control. Release 148 (2010) 177–186.